Journal of Energetic Materials
Publication details, including instructions for authors and subscription information:
http://www.informaworld.com/smpp/title~content=t713770432

Comparison of New and Legacy TATBs

D. Mark Hoffman[a]; Trevor M. Willey[a]; Alexander R. Mitchell[a]; Sabrina C. Depiero[a]
[a] Lawrence Livermore National Laboratory, Livermore, California, USA

To cite this Article Mark Hoffman, D. , Willey, Trevor M. , Mitchell, Alexander R. and Depiero, Sabrina C.(2008) 'Comparison of New and Legacy TATBs', Journal of Energetic Materials, 26: 3, 139 — 162
To link to this Article: DOI: 10.1080/07370650801922195
URL: http://dx.doi.org/10.1080/07370650801922195

Journal of Energetic Materials, 26: 139–162, 2008

ISSN: 0737-0652 print/1545-8822 online
DOI: 10.1080/07370650801922195

Comparison of New and Legacy TATBs

D. MARK HOFFMAN, TREVOR M. WILLEY, ALEXANDER R. MITCHELL, and SABRINA C. DEPIERO

Lawrence Livermore National Laboratory, Livermore, California, USA

Two newly synthesized versions of the insensitive high explosive (IHE) 1,3,5-triamino-2,4,6-trinitrobenzene (TATB) were compared to two legacy explosives currently used by the Department of Energy. Except for thermal analysis, small-scale safety tests could not distinguish between the different synthetic routes. Morphologies of new TATBs were less faceted and more spherical. The particle size distribution of one new material was similar to legacy TATBs, but the other was very fine. Densities and submicron structure of the new TATBs were also significantly different from the legacy explosives and the densities of pressed pellets were lower. Recrystallization of both new TATBs from sulfolane produced nearly hexagonal platelets with improved density and thermal stability.

Keywords: density, morphology, SAXS, TATB, thermal stability, voids

Introduction

Modern Department of Energy (DOE) weapons systems gain enhanced safety from plastic-bonded explosives (PBXs) that

Address correspondence to D. Mark Hoffman, L-282, Lawrence Livermore National Laboratory, Livermore, CA 94550. E-mail: hoffman2@llnl.gov

contain the insensitive high explosive (IHE) 1,3,5-triamino-2,4,6-trinitrobenzene (TATB) bonded together with Kel-F 800, a copolymer of vinylidene fluoride and chlorotrifluoroethylene. Currently, LLNL has limited wet-aminated (WA) TATB reserves for formulation. Although TATB is being synthesized and may soon be commercially available, the synthesis processes have changed and the explosive must be reevaluated. Legacy wet- and dry-aminated (DA) TATB have not been synthesized in the United States in any significant quantity since about 1985. Furthermore, significant quantities of the PBXs based on TATB/Kel-F (LX-17 and PBX 9502) have not been formulated since about 1990 [1]. Over the last few years as part of a Department of Defense Manufacturing Technology Effort, Alliant Tech Systems-Thiokol [2] (ATK) and British Aerospace Engineering (BAE) at Holston Army Ammunition Plant [3] have produced moderate quantities of TATB ($\sim$5-kg batches) with plans to scale up for DOD applications. ATK TATB is polycrystalline with an average particle size of about 40 μm (similar to WA TATB) but BAE TATB is only 5–6 μm (similar to ultrafine).

The subject of this article is characterization of the four TATBs: the new BAE Holston and ATK Thiokol compared to legacy wet-aminated (WA) and dry-aminated (DA) TATB, which are no longer manufactured in the United States. Small-scale safety data on these TATBs are indistinguishable except that newer TATBs decompose thermally about 10°C below the decomposition temperature of dry-aminated TATB, which is about 5°C below that of wet-aminated. The morphology of these TATBs was characterized by scanning electron microscopy. With increasing pressure the density of compression molded disks approached the average density of the corresponding TATB crystals. Ultra-small-angle x-ray scattering (USAXS) measurements on pressed pellets showed different interfacial characteristics for ATK TATB compared to the others. Density distributions of new TATB crystals were substantially less than old crystals as measured using a gradient column. To match characteristics of legacy materials necessitates removal of the impurities and improvement of the crystal structure of these TATBs. To that end, small-scale recyrstallization of BAE and

ATK TATB from sulfolane produced crystals with density and thermal decomposition temperatures comparable to wet-aminated TATB.

Experimental

Legacy wet- and dry-aminated TATB used in these experiments was originally synthesized by Aerojet Corporation, sold to Holston Army Ammunition Plant and given lot numbers 12-03-82-0324-273 and 13-03-85-0307-538, respectively. Sample quantities of these TATBs were obtained by LLNL and given the lot numbers C-090 and C-084. Five hundred grams each of three different lots of Thiokol (ATK) and Holston (BAE) TATB were graciously provided by the Naval Surface Warfare Center at China Lake, CA [4]. All of the tests described in this article used ATK lot TATB001 and BAE lot BAE6E295-001, hereafter referred to as C-562 or C-559, respectively.

All explosives used at LLNL are subjected to impact sensitivity, friction, and spark small-scale safety tests prior to other evaluation or use in prototype devices. Thermal stability is also evaluated using chemical reactivity (CRT) and differential scanning calorimetry (DSC) tests. A thorough critique of various small-scale tests is given elsewhere [5,6].

Morphological comparisons of the various TATBs were made using a LEO 438 VP (variable pressure) scanning electron microscope (SEM). The variable pressure SEM reduces surface charging of an organic sample by allowing a low-pressure atmosphere to pass over the sample to bleed off excess charge. Particle size distributions were determined using the Saturn DigiSizer 5200 laser light scattering apparatus manufactured by Micromeritics Instrument Corporation. Samples of approximately 15 mg of TATB in 2-mL DI water were dispersed with Coulter 1 A surfactant and 3 min of sonication in an external sonicator. The morphology of sulfolane recrystallized TATBs was evaluated using a Zeiss 40-A polarizing microscope under crossed polars with a first-order red plate. Optical micrographs were calibrated against photographs of a stage micrometer at the same magnification with Axiovision software. Further description

of the equipment used in the morphological studies can be found in the manufacturers' instruction manuals [7–9].

A Techne model DC-2 density gradient column was used for all crystal density measurements. The column was immersed in a water bath with temperature controlled to 23 ± 0.05°C. The manufacturer claims density can be estimated to 0.0001 g/cc with this equipment [10]. The gradient was achieved using slow mixing of a high-density aqueous $ZnBr_2$ solution (approximately 2.00 g/cc) into a low-density solution initially about 1.84 g/cc, which was fed into the gradient column. Calibrated glass density beads were added to the column and the height of the center of each bead was measured to within 0.1 cm. A least squares calibration curve for the column was generated from the bead position and its density. Approximately 0.001 g of TATB was immersed in the low-density liquid to wet out the crystals and added to the top of the column with an eye dropper. The crystals were allowed to sink overnight to reach equilibrium density prior to counting. TATB particles within each gradation on the column were counted and the density calculated from the least squares fit of the calibration beads. Several thousand particles were counted in the gradient column. Further description of this apparatus and its application to explosive crystals is given elsewhere [11,12].

Approximately 0.19 g of TATB was compression molded using a Black Hawk press into 1.27-cm-diameter disks approximately 0.08 cm high at pressures between 35 and 200 MPa (5,000–30,000 psi) pressure at ambient for 1 min and released. Pellet densities were calculated from dimensional measurements and weight. The surface of the pressed pellet was examined under epi illumination with differential interference contrast (DIC) inserts in the Zeiss 40-A polarizing microscope [9].

Results and Discussion

Small-Scale Safety Data

Small-scale safety data on the four different types of TATB are given in Table 1. A discussion of these safety tests has been

Table 1
Small-scale safety test results show all synthetic routes produce insensitive HE

TATB	DH 50 (cm)	Friction (kg)	Spark	DSC (Ton)	Tpk
WA	>177.4	>36.0	NS	353	386.9
DA	>177.4	>36.0	NS	348	378.3
ATK	>177.4	>36.0	NS	285	352.7, 368.4
BAE	>177.4	>36.0	NS	310	367.3

presented elsewhere [5,6]. As can be seen from the data, all of these explosives produce no reaction in impact, spark, and friction tests. In Fig. 1, the DSC traces of the new TATBs decompose at 10–15°C lower temperatures than the older TATBs. Wet aminated TATB has the highest decomposition peak temperature (386.9°C), with an onset of about 353°C. This synthetic route produces high-purity TATB [13]. Dry-aminated

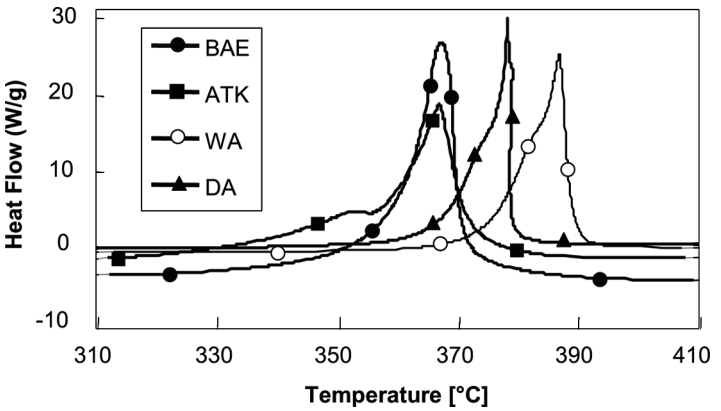

Figure 1. Differential scanning calorimetry (DSC) traces from the four synthetic routes show lower decomposition temperatures for the newer TATBs, apparently due to impurities.

TATB decomposed about 5–8°C lower (378.3°C peak temperature). It is known that DA TATB contains about 0.5% residual NH_4Cl from the synthesis process [14,15]. Scanning electron microscopy reveals micron-size voids where this salt has been extracted from the crystal during washing, but it is currently unclear whether this or smaller size or impurities such as residual NH_4Cl is responsible for the reduction in thermal decomposition temperature. The ATK sample had a second peak at about 352.7°C and the main decomposition peak at 368.4°C. This is significantly lower than their reported peak temperature of 378.1°C [5]. Thiokol reports about 96% purity for their early TATB production, which has been improved to 98% in more recent syntheses. BAE TATB reports purity of 98.5–99.1% and decomposition peak temperatures of 364–368°C, consistent with results given here [6]. They also report that 99.9% pure TATB synthesized at their Bridgewater plant in the UK had decomposition peaks between 389 and 381°C, again consistent with our wet-aminated result. We have found that ultrafine TATB produced by colloidal milling wet-aminated TATB shows a reduction of about 5–7°C in the decomposition peak (around 379–380°C), not enough to account for the 20°C reduction in the new BAE TATB. Although several kinetic studies of TATB with DSC [16–18] have tried to estimate activation energies for thermal decomposition, they contain sparse information on the effects of particle size or impurities. It would appear [19] that there is a relationship between purity, particle size, and decomposition temperature, but further study would be required to determine dependence on these parameters.

Morphologies of TATBs

TATB morphologies were evaluated by scanning electron microscopy (SEM). As can be seen in Fig. 2, SEMs of the various TATBs have very different morphologies. Both new TATBs in Figs. 2b and 2d are spherical aggregates. The ATK TATB large aggregates in Fig. 2b averaged about $77 \pm 16\,\mu m$ and were made up of smaller spherical particles about

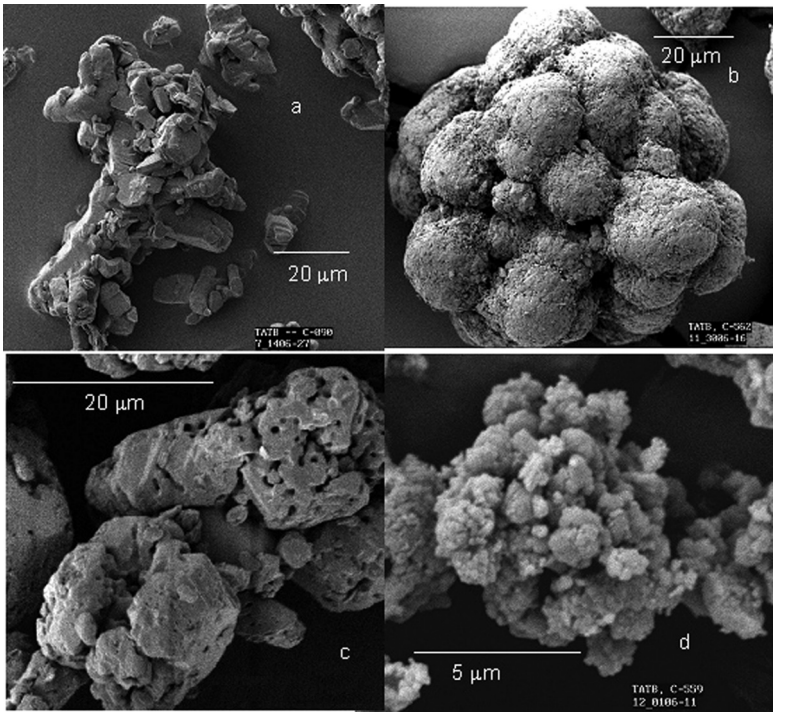

Figure 2. SEMs of (a) wet-aminated TATB; (b) ATK Thiokol TATB; (c) dry-aminated TATB; and (d) BAE Holston TATB.

$28 \pm 8\,\mu m$, which were in turn made up of smaller crystalline aggregates of about $3 \pm 3\,\mu m$. BAE TATB in Fig. 2d was much finer but also composed of spherical aggregates about $5\,\mu m$ across composed of submicron particles of about $0.7 \pm 0.3\,\mu m$. In Fig. 2a, WA TATB shows its characteristic polycrystalline structure, with crystallite sizes near 30–60 µm, along with fines on the order of 5–10 µm. Facets are often observed and steps on the surface have been seen in WA TATB. The classic DA TATB morphology is shown in Fig. 2c [20,21]. Facets of the triclinic unit cell can be seen peppered with holes where the ammonium chloride has been extracted during the final washing cycle.

Density Distributions of TATBs

Densities of TATB were measured using the density gradient technique [22–24]. Theoretical maximum density (TMD) of TATB is 1.937 g/cc [25]. Density distributions of dry- and wet-aminated TATB in Fig. 3 were almost identical, with the mean density of wet-aminated being 1.9173 g/cc or about 98.98% TMD and dry-aminated mean density of 1.9181 g/cc or about 99.02% TMD. It is known [1] that dry-aminated TATB contains approximately 0.5% ammonium chloride from its synthesis route compared to about 0.1% for wet. Since the density of ammonium chloride is about 1.53, the void volume of dry-aminated TATB may be higher than the simplistic estimate given here. Looking at the SEM micrograph of dry-aminated TATB in Fig. 2c would seem to indicate that the 1- to 2-μm holes that cover the surface of the dry-aminated crystals can be wetted and penetrated by the density gradient

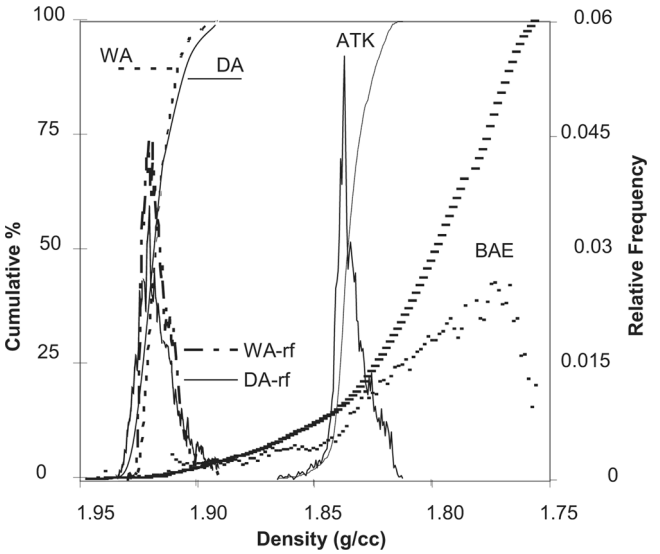

Figure 3. Density distributions in new TATB were much lower than in original wet- and dry-aminated TATB, probably due to impurities and voids.

fluid. Assuming all the voids to be air would imply a void content of about 1%. The Thiokol TATB density distribution maintained the shape of the wet- and dry-aminated distributions but was shifted to lower density. This may imply that the mechanism of void formation is similar in these three samples. The average density (1.8355 g/cc or only 94.75% TMD) was much lower than the legacy TATBs. It is known that ATK and BAE TATBs contain on the order of 2% impurities [2,3]. Although the density of these impurities is not known, it is expected to be comparable or higher than ammonium chloride. Again, the estimate of percentage voids would probably be higher than the simple difference approximation (5.3%). The very fine BAE particle size made the density distribution difficult to measure. As can be seen in Fig. 3, a very broad distribution was found for this TATB with a mean density of 1.8010 g/cc. Near 1.91 g/cc density a group of large particles was observed, above this density until about 1.78 g/cc fine particles increased in number and below 1.78 g/cc a cloud of very fine particles was observed up to nearly the top of the column (1.765 g/cc). The number of particles in the cloud was estimated by counting a region and assuming similar regions contained similar number of particles.

Particle Size Distributions

Light scattering measurements of particle size distribution showed the new TATBs have more fines than WA or DA as shown in Fig. 4. The samples of BAE TATB were finer than ultrafine (UF) TATB by almost a factor of 2, cf, 2.2 μm compared to 3.8 μm average diameter for ultrafine TATB ground in a Sturtevant micronizer [26,27]. Perhaps the spherical aggregates of ATK break down during sonication to produce the extra fines, but the mean particle size was 56 μm, only slightly smaller than B-090 dry-aminated TATB (70 μm). Wet-aminated TATB had an average particle size of approximately 48 μm. So although the morphology is drastically different, ATK is a reasonable particle size match for current stockpile TATBs. BAE claims to have the ability to produce multiple

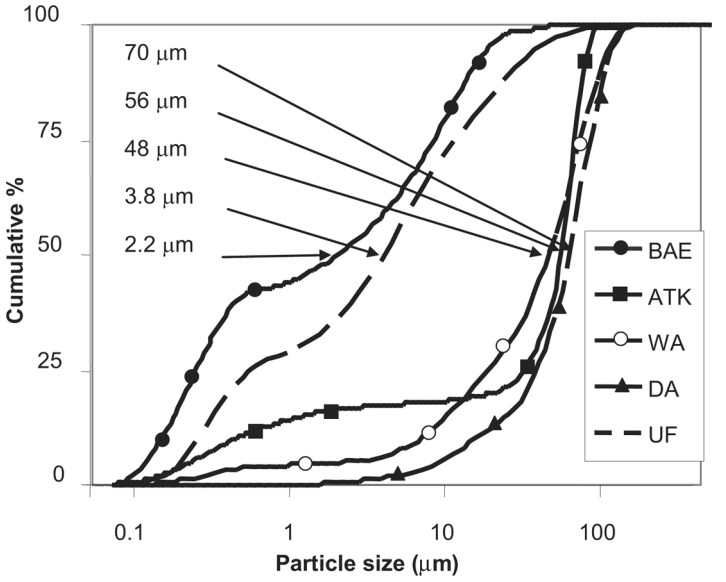

Figure 4. ATK, wet-, and dry-aminated TATB particle size distributions were fairly similar, but BAE TATB was finer than ultrafine TATB made in a Sturtevant mill.

sizes [2], similar to the classes of HMX and RDX, but the sample obtained from NAWS at China Lake was very fine and might initiate better than UF. The relative frequencies of the distributions for ultrafine and BAE TATBs in Fig. 5 clearly show the bimodal nature of these materials.

Characterization of Submicron Structure

Ultra small angle x-ray scattering (USAXS) probes structures from $\sim$10 nm to $\sim$2 μm [28]. Figure 6 presents USAXS from wet-aminated, dry-aminated, Holsten (BAE), and Thiokol (ATK) TATB from small disks pressed at 30,000 psi. Although pressed samples presented here and, to a greater extent, the powders showed multiple scattering, qualitatively the data show a number of interesting characteristics. Scattering occurs

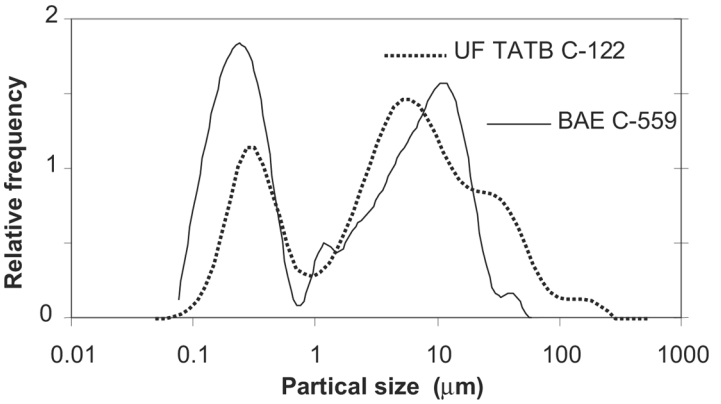

Figure 5. Relative frequency of particles of BAE and ultrafine TATB show the bimodal characteristics of these materials.

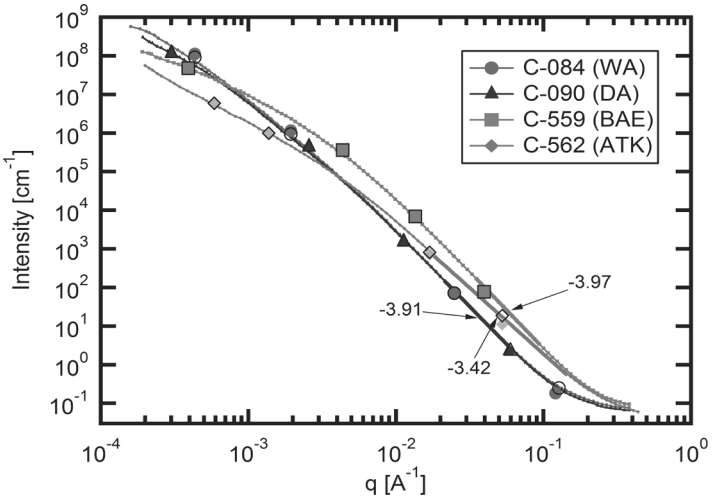

Figure 6. Comparison of ultra-small-angle x-ray scattering of WA (circle), DA (triangle), BAE (square), and ATK (diamond) TATBs from pressed disks show substantial differences between manufacturers.

due to electron density differences and thus cannot distinguish between scattering from particles or voids. In these cases, the calculated volume contributing to the scattering calculated using the invariant [29] is about 5 and 4% for wet- and dry-aminated, 13% for the Holsten, and 4% for the Thiokol TATB. With the exception of the Thiokol, these are much higher than the void volume calculated by density, so we must assume that the observed scattering occurs from both voids and particles.

The Holsten and Thiokol samples have a much larger population of small scatterers (less than $\sim$50 nm) than the wet- and dry-aminated as seen by the more intense scattering intensity at high scattering angle (larger than about $10^{-2}/\text{Å}$). For the Holsten TATB, this is consistent with the smaller crystallites seen in the SEM micrographs of Fig. 2d. The surface area-to-volume ratio calculated from the USAXS is also about one order of magnitude larger in both the Holsten and Thiokol compared to the wet- and dry-aminated TATB.

The clearest scattering difference between the Thiokol and the other TATB samples is the power-law exponent annotated in Fig. 6. For an ideal, two-phase system (i.e., TATB and air) with three-dimensional scatterers, the exponent approaches -4 [29,30]. Wet-aminated (-3.89 to -3.94), dry-aminated (-3.85 to -3.90) ,and even the Holsten (-3.97) are very close to this value, indicating an abrupt interface between TATB and air, consistent with crystalline facets at the interface. Thiokol TATB, however, has an exponent of -3.42. Although different power-law exponents are associated with reduced dimensionality, the exponent seen in the Thiokol case arises from a diffuse or rough fractal-like surface interface [29], as seen in the SEM micrograph in Fig. 2.

Pressing Characteristics

The density, ρ, of $\sim$0.2-g disks of TATB was evaluated as a function of pressing pressure, P, between $35 < \text{P} < 210$ MPa (5,000 to 30,000 psi) for a single, one-minute dwell at ambient. For zero pressure the bulk density of the sample was used. As molding pressure is increased, the part density should approach

the theoretical maximum for the density, ρ_{T}, of the TATB crystal (1.937 g/cc). The percentage of ρ_{T} is

$$\%\mathrm{TMD} = 100\rho./\rho_{\mathrm{T}} \tag{1}$$

Assuming only air is trapped internally and its contribution to the density is negligible, the void volume fraction, $\phi(\mathrm{v})$, would be $1 - \rho/\rho_{\mathrm{T}}$. A schematic diagram of the process is shown as an insert in Fig. 7. The part density as a function of ram pressure for a single one-minute dwell was highest at 200 MPa (30 ksi) in all cases. WA and DA TATB could be pressed to nearly theoretical maximum density (TMD), 99.3 and 99.7%, respectively. ATK TATB could be pressed only to 94.9% TMD and the fine powder BAE TATB would only press to 90.9%. This may be due to the spherical structure of these TATBs and the smaller particle size of BAE. Ultrafine TATB (ground) also does not press to very high density [24]. Table 2 lists the densities and void volume fraction of the different TATBs.

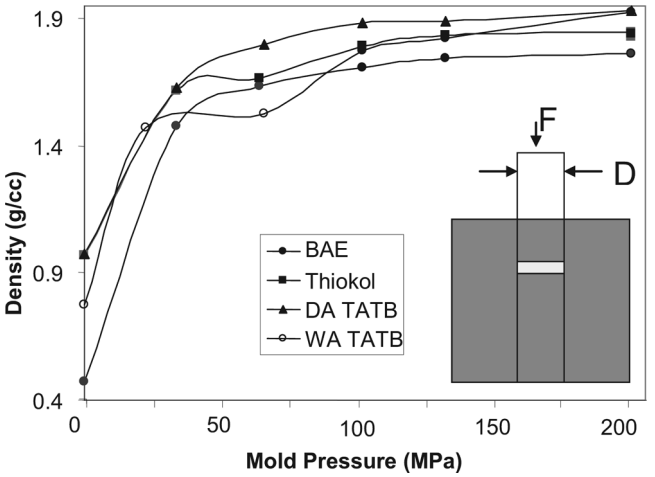

Figure 7. Density as a function of pressure for single dwell ambient pellet of TATB increased slowly as the pressure increased above 5000 psi.

Table 2
Density, ρ, and void volume, ϕ(v), of 0.2-g disks of TATB as a function of pressing pressure, P

P/TATB	ρ (DA)	ϕ (v)	ρ (WA)	ϕ (v)	ρ (ATK)	ϕ (v)	ρ (BAE)	ϕ (v)
0 MPa	0.973	50	0.773	60	0.968	50	0.472	76
35.2	1.629	16	1.473	24	1.617	17	1.475	24
66.9	1.799	7.1	1.524	21	1.662	14	1.634	16
106.2	1.886	2.6	1.772	8.5	1.793	7.4	1.706	12
137.2	1.888	2.5	1.824	5.8	1.832	5.4	1.743	10
208.2	1.933	0.21	1.924	0.67	1.842	5.1	1.761	9.1

Each pressed pellet surface was examined in reflection using differential interference contrast (DIC) microscopy. In some instances it is possible to distinguish intercrystalline interfaces due to differences in refractive indices between crystals [31–33]. Photomicrographs, shown in Fig. 8, were taken at the highest magnification ($\sim$1000 $\times$) and the 20-μm bar in the lower left micrograph is representative for all photos. At the highest pressures, usually TATB crystals are no longer identifiable due to surface damage and flow. At lower pressures an attempt was made to measure crystal dimensions where such structures were observable.

In Fig. 7, the density dependence of wet-aminated TATB with increasing molding pressure was sigmoidal. The DIC micrographs of the pressed pellet at low pressure, first row, first column in Fig. 8, show a rough interface. Since the depth of field is low, out-of-focus regions at low pressure represent depressions or high spots on the surface. The area of the out-of-focus parts of the first micrograph in Fig. 8 (35 MPa) under WA consists of about 12%. This is not very close to the 24% voids estimated from the density difference at this pressure. This would seem to imply that the defects are mainly interstitial crystal packing problems and are fairly large at low mold pressures. At higher pressures plastic deformation allows the polycrystalline aggregates in WA TATB to deform and fill

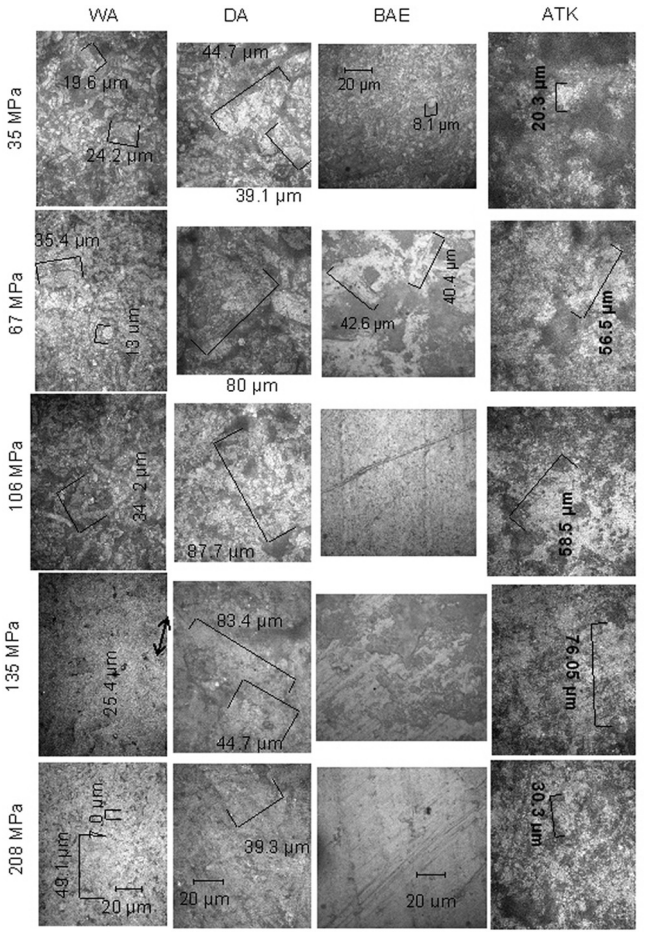

Figure 8. Differential interference contrast micrographs of the surfaces of the various TATBs show increasing plastic deformation with pressure.

the interstitial voids. The WA crystals on the surface begin to coalesce at about 140 MPa (15 ksi). Prior to coalescence, particle size on the surface does not seem to change significantly running between 15 < dia. < 35 µm. This is about 25% smaller that the average particle size of the unpressed WA TATB,

consistent with crystalline fracture and particle size reduction observed in compression molded PBXs [34].

In Fig. 7, the density dependence of dry-aminated (DA) TATB with molding pressure increased asymptotically toward TMD. Judging by the density, the larger crystals of DA TATB packed better than WA TATB at lower pressure although in the high-pressure limit the densities were indistinguishable (1.933 and 1.924 for DA and WA TATB, respectively). These DA crystals withstood the pressure better than WA based on nearly constant crystal dimensions with increasing pressure (compare Fig 8, column 1 with column 2). Some of the DIC images at low molding pressure showed voids on crystal faces parallel to the surface, which were on the order of 1–3 μm, similar in size to the voids observed in the DA TATB SEM in Fig. 2c. The out-of-focus surface area of DA TATB pressed at 35 MPa, 12.6%, compared well with 16% void volume based on density measurements.

The BAE TATB has very low bulk density (0.472 g/cc) compared to all of the other TATBs (0.8 to 0.9 g/cc). The pressing characteristics are shown in Fig. 7. Low pressure increased the density by three times but with increasing pressure only 91% TMD was obtained, the lowest of all pressed pellets. The small particles of the original BAE TATB sample are only observed in DIC micrographs of the disk surface at the lowest pressure (see Fig. 8, column 3). Above 35 MPa (5 ksi) only the marks of the ram surface and large aggregates of unknown origin were observed. These aggregates are not seen at all pressures but could be found in different regions of the surface above 35 MPa (5 ksi). Comparison of the surface-to-volume void content for BAE TATB was not possible because of the small size of the TATB particles. This material cannot be the so-called dirty binder [35,36], since no binder was used to prepare these samples and the idea of rubbled particles being generated seems less likely with these fine particles. With pressure, as expected, these small primary particles seemed to compact well, compared to substantial plastic flow in the TATBs with larger crystals at higher pressures. Densities, unfortunately, do not improve beyond 91% at maximum pressure.

Pressing characteristics of ATK TATB are similar to WA as shown in Fig. 7. The spherical particles seen in the SEM in Fig. 2c are also evident on the pellet surface at low to moderate molding pressure in Fig. 8. At about 20 ksi, the marks of the ram surface are seen in the pellet. The internal structures of the spherical particles appear as the pressure increased. Estimating the out-of-focus area gave 17.3% compared to density void volume of 17.0%, the best comparison of all samples.

Improved Thermal Stability by Recrystallization

The thermal stability and the density distribution of these new TATBs can be improved significantly by rapid recrystallization in sulfolane. Previous attempts at improving crystal quality have used a variety of solvents, including dimethyl sulfoxide, diphenyl ether, solfolane [37,38], nitrobenzene [25], 1,2 dichlorobenzene, benzonitrile, dimethyl formamide, and chlorobenzene [39]. Recently, in an attempt to make fine TATB particles, superacids methane and ethane sulfonic acid and hexamethylphosportriamide were found to dissolve TATB [40]. Sulfolane was selected because of its relatively rapid dissolution of TATB at 190°C and sharp and rapid precipitation characteristics on lowering the temperature to 175°C. Also, a high degree of recovery of TATB was observed for crystallization under these conditions. The new TATB was suspended in sulfolane (1.2% w/v) and rapidly heated with stirring for 4 min when dissolution occurred (∼190°C). The heat source was removed and the resulting solution cooled and stirred with crystallization commencing at ∼175°C. The crystalline suspension was stirred (30 min) and then filtered (∼30°C). The recrystallized TATB was washed with acetone, water, and acetone and dried under vacuum. Yellow, crystalline TATB recoveries varying from 89 to 100% have been obtained.

Polarized optical micrographs of the sulfolane recrystallized TATB from the BAE sample are shown in Fig. 9. These large, triclinic crystals averaged $83 \pm 17\,\mu m$ normal to the [001] axis and many contained what appear to be etch pits or inclusions about $3.4 \pm 0.6\,\mu m$ across. It would seem that one of the BAE

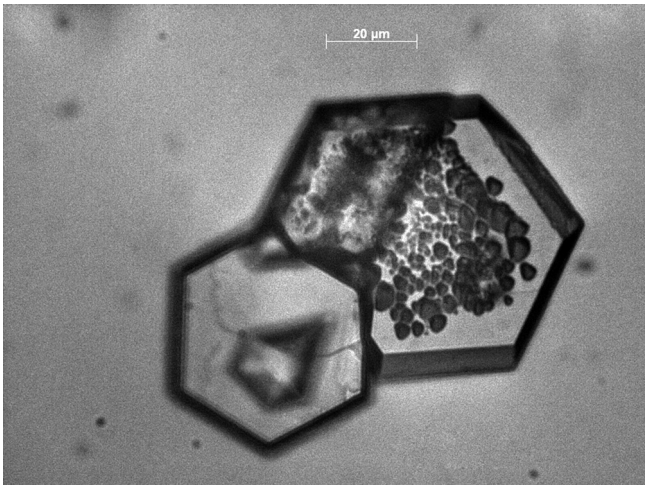

Figure 9. BAE TATB recrystallized in sulfolane showed etch pits or inclusions in many crystals.

impurities from their synthesis route tends to act as a nucleating agent and remain included in the crystal. The peak decomposition temperature in the DSC for these crystals in Fig. 10 increased by 13°C compared to the original BAE TATB in Fig. 2. The bimodal character of the exotherm is often observed in TATB [17] and has been attributed to an autocatalytic first step in the decomposition of TATB but may reflect the influence of impurities on the thermal decomposition.

The ATK recrystallized crystals in Fig. 11 averaged $120 \pm 40\,\mu m$ with lower levels of inclusions than were found in the BAE crystals and what appear to be dislocations in nicely formed triclinic crystals. Again the DSC decomposition temperature increased after recrystallization. In this case, the decomposition peak was 0.6°C higher than the legacy WA sample, also shown in the figure. Further optimization of a short residence time recrystallization procedure would be of interest since it lends itself to scale-up but this was not pursued here. Average density of the recrystallized ATK TATB increased from 1.835 to 1.9140 g/cc, comparable to wet- and dry-aminated densities.

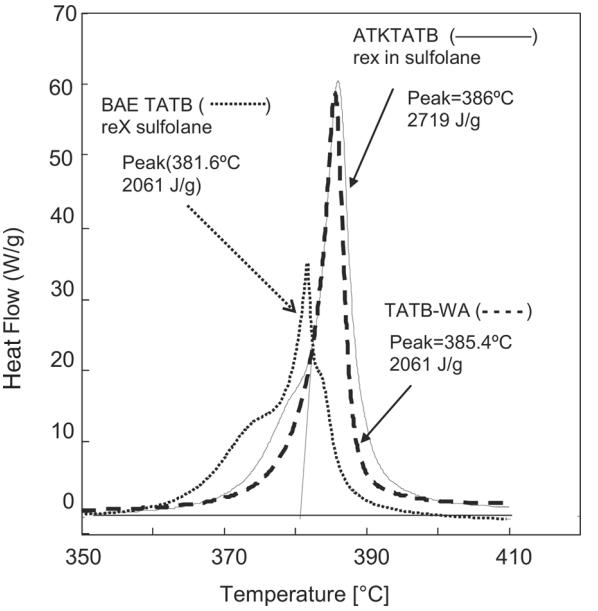

Figure 10. Thermal decomposition of BAE (dotted line) and ATK (solid line) TATBs recrystallized from sulfolane compared to wet-aminated TATB (dashed line) showed increased peak temperature compared to original samples.

Conclusions

Significant differences between new and legacy TATBs were found in this study. Although the particle size distributions, as measured by light scattering, for WA, DA, and ATK TATBs were similar, the morphology, thermal stability, density, and submicron structure were significantly different. BAE TATB had much smaller particles than the legacy TATBs. How the differences in ATK and BAE TATB will affect the formulation and performance of TATB-based PBXs such as LX-17 and PBX 9502 compared to legacy material is currently under study, but results are not expected to be similar. Different morphologies and surface characteristics are expected to alter processing characteristics in the Holston slurry coating reactor.

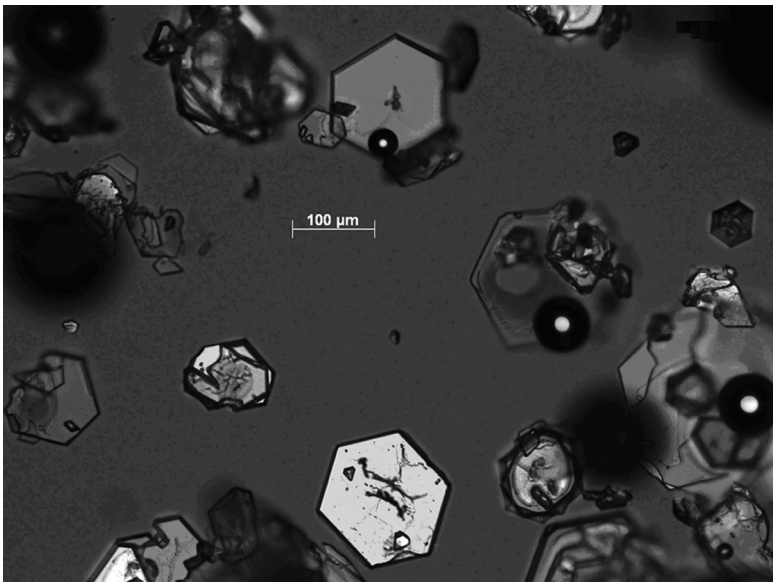

Figure 11. ATK TATB recrystallized from sulfolane produced these large platelets.

Molding powder size, bulk density, and granularity may be affected. Pressing characteristics and mechanical properties are expected to change. Lower densities of the new TATBs are expected to alter initiation characteristics, probably making the PBXs easier to initiate. Reduced thermal stability may alter cook-off characteristics. Experiments are ongoing or planned to address some of these questions.

Acknowledgments

We thank Tim Mahoney at China Lake for supplying the new TATB samples. George Overturf, John C. Estill, and Bill Mclean provided funding for this work in conjunction with engineering efforts of Peter Raboin and Angela Cook. Pat Lewis ran the light scattering measurements for particle size distributions. Heidi Turner made the thermal analysis measurements. Aaron Fontes made the density distribution measurements.

We acknowledge Lisa Lauderbach and Tony van Buuren of LLNL, and Jan Ilavsky, Advanced Photon Source, Argonne National Laboratory, for assistance in performing USAXS experiments. Use of the Advanced Photon Source was supported by the U.S. Department of Energy, Office of Science, Office of Basic Energy Sciences, under Contract No. DE-AC02-06CH11357. Work performed under the auspices of the U.S. DOE by University of California, Lawrence Livermore National Laboratory under Contract @-7405-Eng-48.The project 06-SI-005 was funded by the Laboratory Directed Research and Development Program at LLNL.

Disclaimer

References

[1] Colville, J. C. 1992. *LX-17 and LX-10 Test Data SR-92-03.* Pantex Plant, Amarillo, TX.

[2] Sleadd, B. 2006. *Synthesis and Scale-Up of Sym-Triaminotrinitrobenzene at Holston Army Ammunition Plant.* IM&EM Technology Symposium, April 24–27, 2006, Bristol, UK.

[3] Velarde, S. 2006. *Pilot Plant Synthesis of Triaminotrinitrobenzene (TATB)*. IM&EM Technology Symposium, April 24–27, 2006, Bristol, UK.
[4] Mahoney, T. 2006. Private Communication, June 2006.
[5] Mellor, A. M., T. L. Boggs, J. Covino, C. W. Dickenson, D. Dreitzler, L. B. Thorn, R. B. Frey, P. W. Gibson, W. E. Roe, M. Kirshenbaum, and D. M. Mann. 1988. Hazard initiation in solid rocket and gun propellants and explosives. *Progress in Energy and Combustion Science*, 14: 213.
[6] Simpson, L. R. and M. F. Foltz. 1996. *LLNL Small-Scale Friction Sensitivity (BAM) Test, UCRL-ID-124563*; 1995. *LLNL Small-Scale Drop-Hammer Impact Sensitivity Test, UCRL-ID-119665*; 1999. *LLNL Small-Scale Static Spark Machine: Static Spark Sensitivity Test, UCRL-ID-135525*. Livermore, CA: Lawrence Livermore Laboratory.
[7] 1997. *LEO 435VP Operators Manual*. v. 3.0. Cambridge, England: Leo Electron Microscopy, Ltd.
[8] 2002. *Saturn DigiSizer 5200 Operators Manual 520-42801-01*. Norcross, GA: Micromeritics Instrument Corporation.
[9] 2002. *Zeiss Axioskop 40 Pol Polarizing Microscope Operating Manual B 46-0016*. Goettingen, Germany: Carl Zeiss Light Microscopy.
[10] 1988. *Techne Operating Manual*. Princeton, NJ: Techne, Inc.
[11] Hoffman, D. M. 2003. Voids and density distributions in 2,4,6,8,10,12-hexanitro-2,4,6,8,10,12-hexaazaisowurtzitane (CL-20) prepared under various conditions. *Propellants, Explosives, Pyrotechnics*, 28(4): 194–200.
[12] Hoffman, D. M. 2001. Density distributions in cyclotrimethylenetrinitramines (RDX). Paper read at the 38th JANNAF Meeting, Destin, Florida, April 8–12, 2002.
[13] Benziger, T. M. 1977. Method for the production of high-purity triaminotrinitro benzene. U. S. Patent No. 4,032,377.
[14] Bellamy, A. J., S. J. Ward, and P. Golding. 2002. A new synthetic route to 1,3,5-triamino-2,4,6-trinitrobenzene (TATB). *Propellants, Explosives, Pyrotechnics*, 27: 49–58.
[15] Ott, D. G. and T. M. Benziger. 1987. Preparation of 1,3,5-triamino-2,4,6-trinitrobenzene from 3,5-dichloroanisole. *Journal of Energetic Materials*, 5: 343–354.
[16] Rogers, R. N., J. L. Janney, and M. H. Ebinger. 1982. Kinetic-isotope effects in thermal explosions. *Thermochimica Acta*, 59: 287–298.

[17] Catalano, E. and P. C. Crawford. 1983. An enthalpic study of the thermal decomposition of unconfined TATB. *Thermochimica Acta*, 61: 23–36.
[18] Zeman, S. 1993. The thermoanalytical study of some amino-derivatives of 1,3,5-trinitrobenzene. *Thermochimica Acta*, 216: 157–168.
[19] Koerner, J., J. Maienschein, A. Burnham, and A. Wemhoff. 2007. ODTX measurements and simulations on ultra fine TATB and PBX 9502. Paper read at symposium, NATAS 35th Annual Conference, August 26–29, 2007, East Lansing, MI.
[20] Cady, H. H. 1986. Microstructural differences in TATB that result from manufacturing techniques. Paper read at the 17th International ICT Conference, June 1986, Karlsruhe, Germany.
[21] Duncan, A. A. 1991. *TATB Powder Characteristics of Holston-Formulated PBX 9502, MHSMP-91-18*. Mason & Hanger Pantex Plant, Amarillo, TX.
[22] Low, B. W. and F. M. Richards. 1952. The use of the gradient tube for the determination of crystal densities. *Journal of the American Chemical Society*, 74: 1660.
[23] Tung, L. H. and W. C. Taylor. 1956. An improved method of preparing density gradient tubes. *Journal of Polymer Science*, 21: 144.
[24] ASTM D 1505-85. 1985. *Standard Test Method for Density of Plastics by the Density-Gradient Technique*. West Conshohocken, PA: ASTM, International.
[25] Cady, H. H. and A. C. Larson. 1965. The structure of 1, 3, 5-triamino-2,4,6-trinitrobenzene. *Acta Crystallographica*, 18: 485–496.
[26] Chambers, D. M. 2000. *Analysis of UF TATB by Ultrasonic Equilibrium Head Space Analysis, UCRL-ID-140673*. Livermore, CA: Lawrence Livermore Labs.
[27] Golopol, H. 1982. *Ultrafine TATB Aging Study, UCRL-88018*. Livermore, CA: Lawrence Livermore Labs.
[28] Ilavsky, J., P. Jemian, A. J. Allen, and G. G. Long. 2004. Versatile USAXS (Bonse-Hart) facility for advanced materials research, Paper presented at symposium, Synchrotron Radiation Instrumentation: Eighth International Conference.
[29] Roe, R.-J. 2000. *Methods of X-ray and Neutron Scattering in Polymer Science*. Oxford, UK: Oxford University Press.
[30] Willey, T. M., T. van Buuren, J. R. I. Lee, G. E. Overture, J. H. Kinney, J. Handly, B. L. Weeks, and J. Ilavsky. 2006. Changes in pore size distribution upon thermal cycling of

TATB-based explosives measured by ultra-small angle x-ray scattering. *Propellants, Explosives, Pyrotechnics*, 31(6): 466.

[31] Danz, R. and P. Gretscher. 2005. C-DIC: A new microscopy method for rational study of phase structures in incident light arrangement. *Thin Solid Films*, 462–463: 257–262.

[32] Sazaki, G., K. Tsukamoto, S. Yai, M. Okada, and K. Nakajima. 2005. In situ observation of dislocations in protein crystals during growth by advanced optical microscopy. *Crystal Growth & Design*, 5: 1729–1735.

[33] Johnston, A. P. R., A. N. Zelikin, L. Lee, and F. Caruso. 2006. Approaches to quantifying and visualizing polyelectrolyte multilayer film formation on particles. *Analytical Chemistry*, 78: 5913–5919.

[34] Duncan, A. 2003. *Powder Characterization Seminar Notes*. Amarillo, TX: BWXT Pantex.

[35] Peterson, P. D. and D. J. Idar. 2005. Microstructural differences between virgin and recycled lots of PBX 9502. *Propellants, Explosives, Pyrotechnics*, 30(2): 88.

[36] Skidmore, C. B., D. S. Phillips, and N. B. Crane. 1997. Microscopical examination of plastic bonded explosives. *Microscope*, 45(4): 127–136.

[37] Foltz, M. F., J. L. Maienschein, and L. G. Green. 1996. Particle size control of 1,3,5-triamino-2,4,6-trinitrobenzene by recrystallization from DMSO. *Journal of Materials Science*, 31(7): 1741–1750.

[38] Foltz, M. F., D. L. Ornellas, P. F. Pagoria, and A. R. Mitchell. 1996. Recrystallization and solubility of 1,3,5-triamino-2,4,6-trinitrobenzene in dimethyl sulfoxide. *Journal of Materials Science*, 31(7): 1893–1901.

[39] Mitchell, A. R. 2006. unpublished results.

[40] Talawar, M. B., A. P. Agarwal, A. Anniyappan, G. M. Gore, S. N. Asthana, and S. Venugopalan. 2006. Method for preparation of fine TATB (2–5 μm) and its evaluation in plastic bonded explosive (PBX) formulations. *Journal of Hazardous Materials*, 137(3): 1848–1852.